Dalton Transactions

Accepted Manuscript

This is an *Accepted Manuscript*, which has been through the RSC Publishing peer review process and has been accepted for publication.

Accepted Manuscripts are published online shortly after acceptance, which is prior to technical editing, formatting and proof reading. This free service from RSC Publishing allows authors to make their results available to the community, in citable form, before publication of the edited article. This *Accepted Manuscript* will be replaced by the edited and formatted *Advance Article* as soon as this is available.

To cite this manuscript please use its permanent Digital Object Identifier (DOI®), which is identical for all formats of publication.

More information about *Accepted Manuscripts* can be found in the **Information for Authors**.

Please note that technical editing may introduce minor changes to the text and/or graphics contained in the manuscript submitted by the author(s) which may alter content, and that the standard **Terms & Conditions** and the **ethical guidelines** that apply to the journal are still applicable. In no event shall the RSC be held responsible for any errors or omissions in these *Accepted Manuscript* manuscripts or any consequences arising from the use of any information contained in them.

Synthesis of porous upconverting luminescence α-$NaYF_4$:Ln^{3+} microspheres and their potential application as carriers

Changjian Lv, Weihua Di*, Zhihe Liu, Kezhi Zheng, and Weiping Qin*

State Key Laboratory on Integrated Optoelectronics, College of Electronic Science and Engineering, Jilin University, Changchun 130012, People's Republic of China.

* Corresponding authors: 2699 Qianjin Street, Changchun 130012, China. E-mail: whdi@jlu.edu.cn (W. Di); wpqin@jlu.edu.cn (W. Qin) Tel: 86-431-85168240-8325, Fax: 86-431-85168240-8325

The present work reported a self-sacrificed template strategy to synthesize porous α-$NaYF_4$ microspheres via the reaction of as-prepared $Y(OH)CO_3·H_2O$@SiO_2 with NH_4F and $NaNO_3$ solutions. XRD, SEM, TEM and N_2 adsorption-desorption measurements were used to characterize the resulting product. The surface SiO_2 shell was indicated to play a vital role in the size and shape control and porosity formation. Possible reaction mechanism was explored in terms of a surface-protected etching and ion-exchange reaction process. To explore their application potential, the storage and release behavior of Rhodamine 640 dye in the porous α-$NaYF_4$ microspheres was investigated, showing a relatively high loading efficiency and a sustained release ratio. Under near-infrared (NIR) irradiation, porous α-$NaYF_4$ microspheres doped with lanthanide ions showed typical upconverting luminescence characteristics that can convert NIR photons to ultraviolet/visible photons. The above features and properties indicate that our present porous upconverting luminescence particles are promising in biological applications as luminescence imaging agents and drug carriers.

1. Introduction

Mesoporous nanomaterials are of great interest in many current areas of technology because of their predominate properties including low density, large specific area, surface permeability and encapsulation ability.[1–5] These specific features of mesoporous materials allow their potential applications, such as in catalysis,[6] sensing,[7] water treatment,[8] waste removal,[9] especially drug delivery and biological labeling and imaging.[10–20]

Currently, the synthetic strategies for the fabrication of porous/hollow structures mostly by well-established approaches involve the utilization of various removable templates, including soft ones such as surfactants, emulsion droplets, micelles, vesicles, ionic solvents and gas bubbles,[21–23] and hard ones, such as polymers, silica, carbon, metal oxides and metallic cores.[24–27] In general, the template-based synthetic methods involve multistep procedures including template removal, and sometimes require stringent synthesis conditions. In some cases, some toxic surfactants or

solvents are needed to add into the reaction system, which renders the final material with significant toxicity.[28] Nowadays much attention has been focused on the newly emerging methods based on self-sacrificial templating synthesis which has significant advantages that it can avoid template removal and simultaneously obtain the controllable and uniform morphologies compared to hard or soft templates.[29–38]

The upconversion luminescence materials, especially lanthanide-doped fluoride systems (e.g. $NaYF_4$ and YF_3), can efficiently convert lower energy photons into higher energy photons through sequential absorption and energy transfer by the use of physically existing intermediary energy states of lanthanide ions.[39–41] They have been recognized as one of the most potential materials in biological applications because of their characteristic advantages such as high signal-to-noise ratio, weak autofluorescence background, large penetration depth, low toxicity and high chemical stability.[42–48] Such superior chemicophysical properties, simultaneously combined with the mesoporous feature, can endow the resulting material with multiple capabilities such as optical imaging and drug storage and release.[49,50]

Consequently, much investigation has been performed on the synthesis of upconverting luminescence agents and their potential applications in biology.[51–53] However, as far as we know there are few researches regarding hollow or porous structured fluoride materials as upconverting luminescence host matrix. Zhang *et al.* reported the preparation of hollow α-$NaYF_4$ spheres via an ion-exchange reaction method.[54] They first synthesized the precursor $Y(OH)CO_3{\cdot}H_2O$ spheres by a homogenous precipitation method and Y_2O_3 was obtained via the precursor calcination, then was reacted with HF and NaF solution by a hydrothermal process, in which HF was not only used as F source, but also acted as a corrosion agent of the precursor Y_2O_3 to generate Y^{3+} ions. However, HF is terribly harmful to the environment and researchers' health during the materials synthesis process and the calcination required also results in large energy consumption.

Herein, we aim to explore an environment-friendly and energy-saving strategy to prepare porous α-$NaYF_4$:Ln^{3+} particles by using $Y(OH)CO_3{\cdot}H_2O$ microspheres coated with SiO_2 as a self-sacrificed template. Initially, the as-prepared bared $Y(OH)CO_3$

microspheres were used as templates to react with NH_4F and $NaNO_3$ solutions by a hydrothermal process. Consequently, we found that the use of bared $Y(OH)CO_3·H_2O$ microspheres as template results in the size increase, size distribution inhomogeneity and no porosity formation for the final products. Interestingly, while $Y(OH)CO_3·H_2O$ microspheres were coated with a thin layer of silica to subsequently react with NH_4F and $NaNO_3$ under the same reaction conditions with the former, we found that, in this modified way, the final products can maintain original size, shape and homogeneity, and also show the porous structure in each single newly formed microsphere. The reaction mechanism was explored on the basis of the above experimental results. To explore their application potential, we investigated the storage and release behavior of Rhodamine 640 dye in the finally obtained porous α-$NaYF_4$ microspheres, exhibiting a relatively high loading efficiency and a sustained release ratio. While doped with (Yb, Tm) or (Yb, Er) ions pair, the porous α-$NaYF_4$ shows upconverting luminescence characteristics upon NIR light excitation, *i.e.*, the conversion of NIR photons to ultraviolet (UV)/visible ones. These features and properties indicate their potential applications in drug carriers and upconverting luminescence imaging agents.

2. Experimental section

2.1. Chemicals.

Analytical grade $Y(NO_3)_3·6H_2O$, $Yb(NO_3)_3·6H_2O$, $Tm(NO_3)_3·6H_2O$, $Er(NO_3)_3·6H_2O$, $CO(NH_2)_2$ (urea), NH_4F, $NaNO_3$, ethanol, tetraethoxysilane (TEOS), ammonia aqueous (28 wt%), Rhodamine 640 (Rh 640)were obtained from Beijing Chemicals Reagents, China. Deionized water was used throughout. All other chemical reagents were of analytical reagent grade.

2.2. Preparation of $Y(OH)CO_3$ colloidal precursors.

The monodisperse $Y(OH)CO_3$ microspheres were prepared via a urea-based homogeneous precipitation process according to the literatures published previously.[55,56] In a typical process, 3 mmol of $Y(NO_3)_3$ and 18.018 g of urea were dissolved in 300 mL of deionized water. The above solution was first homogenized

under magnetic stirring at room temperature for 2 h, then was heated to 90 °C and maintained at this temperature for 2.5 h in the oil bath. The obtained precipitates were separated by centrifugation and washed with deionized water and ethanol several times. Finally, the products were dried in oven at 80 °C for 10 h. The Yb^{3+}/Ym^{3+} and Yb^{3+}/Er^{3+} co-doped $Y(OH)CO_3$ samples were prepared by the same synthesis procedure with a molar ratio of Y:Yb:Tm = 79:20:1 and Y:Yb:Er = 80:18:2, respectively.

2.3. Preparation of core-shell $Y(OH)CO_3@SiO_2$ particles.

The core-shell $Y(OH)CO_3@SiO_2$ microspheres were prepared via a modified sol-gel process according to our previously published literature.[57] In a typical procedure, 50 mg of as-prepared $Y(OH)CO_3:Ln^{3+}$(Ln=Yb/Tm or Yb/Er) microspheres were well dispersed in a mixture of 80 mL of ethanol and 20 mL of deionized water by ultrasonic treatment. Then 60 μL of TEOS dissolved in 20 mL of ethanol was added into the above solution drop by drop, followed by 1.0 mL of concentrated ammonia aqueous solution (28 wt%). The total solution was continuously stirred at room temperature for 24 h and incubated for 6 h. The resulting products were collected by centrifugation and washed with deionized water and ethanol several times, and then dried in the air at 80 °C for 12 h.

2.4. Synthesis of porous α-$NaYF_4$ and Ln-doped α-$NaYF_4$ microspheres.

Porous α-$NaYF_4$ microspheres were synthesized by using $Y(OH)CO_3@SiO_2$ prepared above as precursors. In a typical procedure, 50 mg of the as-prepared $Y(OH)CO_3@SiO_2$ precursors were dispersed into 15 mL of deionized water by ultrasonic treatment for 0.5 h to obtain uniform suspension. Then 64 mg of NH_4F and 127 mg of $NaNO_3$ were dissolved in 15 mL of deionized water by stirring and added into the above $Y(OH)CO_3@SiO_2$ colloidal suspension. After additional agitation for 0.5 h, the mixing solution was transferred into a 30 mL Teflon-lined autoclave and heated to 100 °C for 3 h. After the autoclave was cooled down to room temperature naturally, the obtained precipitates were collected by centrifugation and washed with deionized water and ethanol several times, and then dried in the air at 80 °C for 12 h. Yb^{3+}/Er^{3+} and Yb^{3+}/Tm^{3+} ion pairs-doped α-$NaYF_4$ samples were prepared by

replacing a fraction of $Y(NO_3)_3$ by (Yb, Er)$(NO_3)_3$ or (Yb, Tm)$(NO_3)_3$ under the same conditions as that for the preparation of undoped α-$NaYF_4$ sample.

For comparison, the $Y(OH)CO_3$ colloidal precursors without silica coating was used as precursors to synthesize α-$NaYF_4$ spheres while the other reaction conditions keep the same as the case of $Y(OH)CO_3$@SiO_2 precursors as precursors.

2.5. Storage and release of fluorescence dye.

Rhodamine 640 (Rh 640) was chosen as a model dye to investigate the storage and release behavior of the present porous structured α-$NaYF_4$. In a typical route, 8 mg porous α-$NaYF_4$ particles were added into 15 mL Rh 640 aqueous solution (contains 150 μL of 1000 ppm Rh 640 original aqueous solution). The mixture was shaken under magnetic stirring at room temperature in dark conditions. At selected time intervals, a certain volume of supernatant solution obtained by centrifugation was taken out and transferred to a quartz cuvette for the detection of the absorption of Rh 640 solution using UV-vis spectrophotometer, and then put back in the aqueous solution. Finally, the particles were separated by centrifugation and washed with deionized water.

To check the release of Rh 640 dye, the above-prepared dye-loaded α-$NaYF_4$ particles were immersed in distilled water and shaken at 100 rpm. At certain time intervals, 5 mL of the solution were taken out by centrifugation to test the concentration of released Rh 640 dye and fresh distilled water (5 mL) was added to the tube containing the dye-loaded particles.

2.6. Characterizations.

The crystal structure and phase purities of the products were defined by a Rigaku RU-200b X-ray powder diffraction (XRD) with nicked-filtered Cu-K α radiation (λ = 1.5604 Å). The operation voltage and current were 40 kV and 200 mA, respectively. The 2θ angle ranges from 10° to 70°. The size and morphology of the as prepared samples were further observed by a transmission electron microscopy (TEM) (H-600, 100 kV) and a scanning electron microscopy (SEM, JEOL JSM-7500F). The high-magnification and high-resolution TEM images, energy dispersive X-ray spectroscopy (EDX) spectrum and the selected-area electron diffraction (SAED)

pattern were tested by a field emission transmission electron microscopy (FETEM) (Tecnai G^2 F20, 200 kV). Fourier transform infrared (FT-IR) spectra (Mattson 5000) of the samples were measured in the range of 4000-500 cm^{-1} in transmission mode. The pellets were prepared by adding 0.8 mg of the sample powder to 80 mg of KBr. The powders were mixed homogeneously and compressed at a pressure of 10 kPa to form transparent pellets. N_2 adsorption-desorption isotherms were obtained on a Micromeritics ASAP 2420 apparatus. The samples were degassed at 523 K and 10^{-6} Torrr for 10 h prior to measurement. The absorption spectra of the fluorescence dye solution were detected by the 4802 UV-vis double beam spectrophotometer. Upconversion emission spectra were recorded with Hitachi F-4500 fluorescence spectrophotometer (1.0 nm for spectral resolution and 400 V for PMT voltage) equipped with a power-controllable 980 nm continuous laser diode as excitation source. The upconversion spectra were recorded under identical conditions in order to compare their relative emission intensities.

3. Results and discussion

3.1. Characterizations of $Y(OH)CO_3·H_2O$ and $Y(OH)CO_3·H_2O@SiO_2$ microspheres.

The $Y(OH)CO_3·H_2O$ microspheres were synthesized as precursors via a urea-based homogeneous precipitation process. The urea-based precipitation is a simple and general route for the preparation of rare earth hydroxylcarbonate that was first developed by Matijevic and his co-workers.[55] Urea was introduced as a precipitation agent, which can decompose into the OH^- and CO_3^{2-} under elevated temperature (>83 °C) for the precipitation with the rare earth cations.[55,57] The SEM and TEM images presented in Fig. 1a–c show that the as-prepared $Y(OH)CO_3·H_2O$ particles are spherical, uniform and monodispersed with an average diameter of approximately 260 nm. The spherical and size-uniform morphology of the particles benefits their subsequent surface modifications.[57,58] FT-IR spectrum (Figure S1, Supporting Information), the thermogravimetric analysis (Figure S2, Supporting Information) and the elemental analysis (Table S1, Supporting Information) confirmed that the

chemical composition of as-prepared precursor is $Y(OH)CO_3 \cdot H_2O$ (written as $Y(OH)CO_3$ below for convenience).

The core-shell $Y(OH)CO_3@SiO_2$ particles were prepared via a modified sol-gel process as described in the experimental section. The particles maintain spherical shape and good dispersion after coating (Fig. 1d–f). The typical core-shell structure can be distinctly seen by TEM due to their different electron contrasts for the cores and shells (Fig. 1f). The dark core and gray shell correspond to $Y(OH)CO_3$ and SiO_2 layer, respectively. We can see that the SiO_2 layer is uniform around the cores and the diameter is about 8 nm. The sol-gel process allows for a homogeneous and complete coating around each spherical $Y(OH)CO_3$ particle and no separated SiO_2 particles were formed. From FTIR spectrum, we also detected the vibration of Si–O, confirming the presence of SiO_2 shells (Figure S1, Supporting Information). The easy growth of the homogeneous silica shell on the $Y(OH)CO_3$ particles could be attributed to the composition of the $Y(OH)CO_3$ particles. As a matter of fact, due to the hydrated phase and the presence of hydroxyl groups of as-prepared $Y(OH)CO_3$ particles, TEOS can easily react with the surface of the core particles forming a first silica monolayer on top of which the silica shell can easily grow.[57]

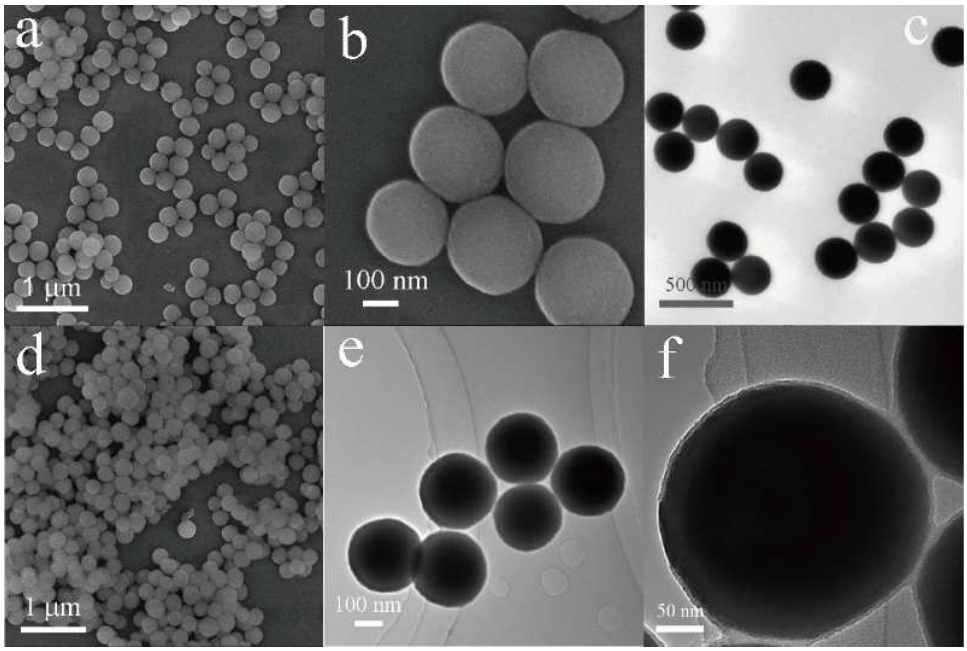

Fig. 1 SEM (a, b) and TEM (c) images of as-prepared precursor $Y(OH)CO_3 \cdot H_2O$; SEM (d)

and TEM (e, f) images of the reaction templates $Y(OH)CO_3@SiO_2$.

3.2. Characterizations of porous α-$NaYF_4$ spheres.

The product $NaYF_4$ was synthesized via a hydrothermal process by using the as-prepared $Y(OH)CO_3@SiO_2$ microspheres as self-sacrificed templates. The crystal structure and phase purities of the products were checked by XRD. Fig. 2 presents the XRD patterns of the as-prepared template $Y(OH)CO_3@SiO_2$ microspheres and the final product synthesized by the reaction of $Y(OH)CO_3@SiO_2$ with NH_4F and $NaNO_3$, respectively. The as-prepared template $Y(OH)CO_3@SiO_2$ is amorphous, while all the diffraction peaks of the final product can be readily indexed to the cubic phase $NaYF_4$ (α-$NaYF_4$, JCPDS # 06-0342, Fig. 2b).

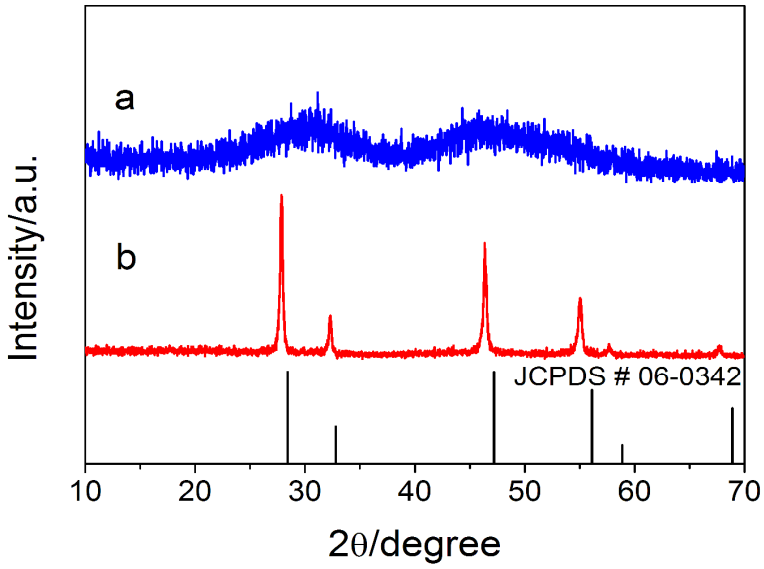

Fig. 2 XRD patterns of (a) the as-prepared template $Y(OH)CO_3@SiO_2$ and (b) the final product $NaYF_4$ synthesized by using $Y(OH)CO_3@SiO_2$ as templates. The standard data of cubic $NaYF_4$ (JCPDS # 06-0342) was used as reference.

The size and morphology of the product were characterized by SEM observations. Fig. 3(a, b) shows the FESEM images of the obtained product. We can see that the particles synthesized via self-sacrificed template method are monodispersed and almost maintain the spherical shape with the original size of templates. The difference is that each microsphere is constituted of numerous nanoparticles that are arranged

closely with each other (Fig. 3b). The interior voids can be clearly observed from several broken spheres (Fig. 3b and its inset), demonstrating a hollow structure.

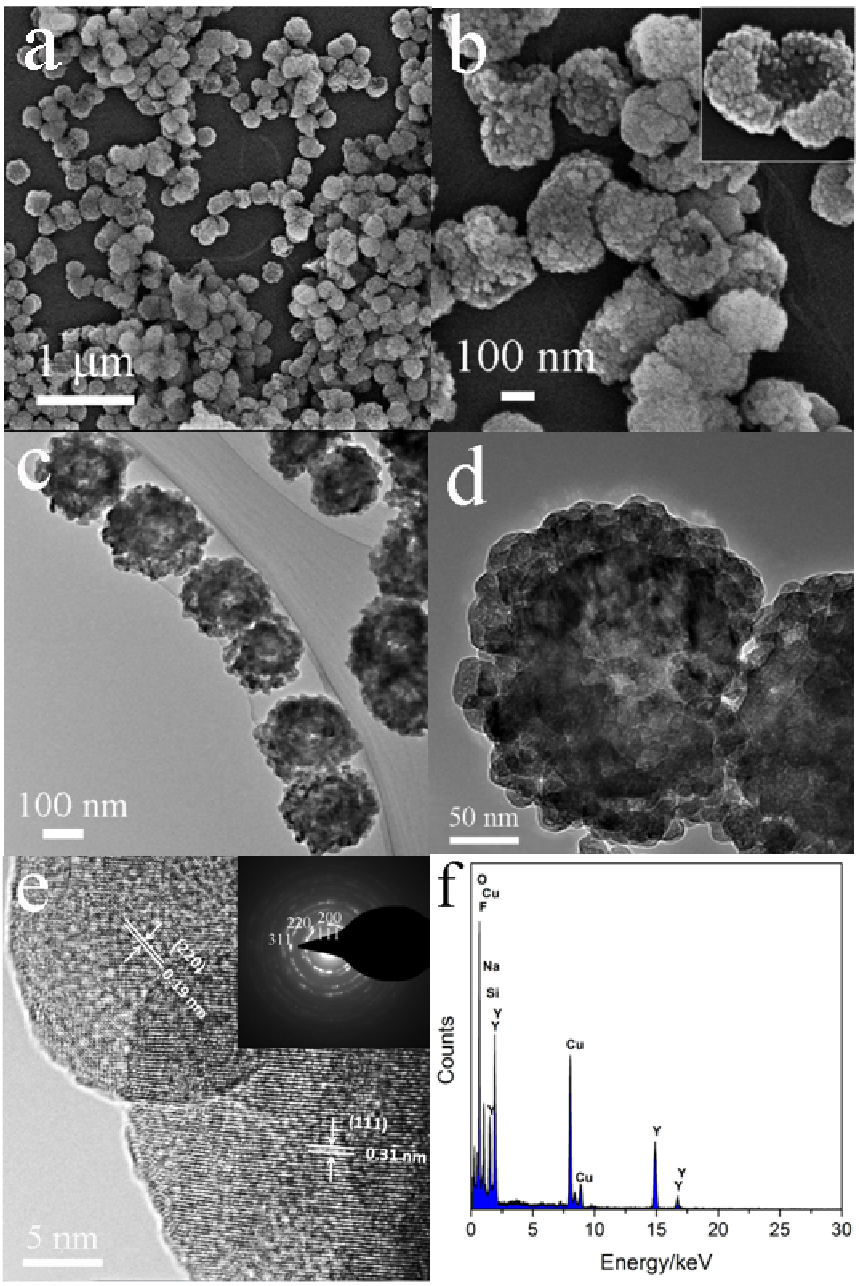

Fig. 3 SEM images(a, b), low- and high-magnification TEM (c, d, e) images and EDX spectrum (f) of porous α-$NaYF_4$ microspheres. SAED pattern was shown in the inset of Figure e.

TEM images displayed in Fig. 3c–e further characterize the size and morphology of the obtained product α-$NaYF_4$. The samples are primarily constituted of several

microspheres with an almost unchanged size, a homogeneous size distribution and a good dispersion. Each primary spherical particle is constituted of tens of nanoparticles with a size of 10–20 nm. These nanoparticles are randomly arranged but distributed homogenously throughout the whole large particle, and the mesopores were created among these small-sized α-$NaYF_4$ nanoparticles, which were proved by many light spots observed in Fig. 3(c, d).

Fig. 3e shows the high-resolution TEM (HRTEM) image and selected-area electron diffraction (SAED) pattern of the resulting α-$NaYF_4$ microspheres. The HRTEM image reveals clear lattice fringes with interplanar spacing of 0.31 nm and 0.19 nm ascribed to the (111) and (220) crystal plane of α-$NaYF_4$, respectively. In the SAED pattern, the strong concentric ring patterns can be indexed to the (111), (200), (220), (311) planes of cubic $NaYF_4$ phase, respectively, and demonstrate its polycrystalline nature. Fig. 3f shows the EDX spectrum of the sample. The atom ratio of Na, Y and F was 12.83: 13.36: 56.04, which is close to the stoichiometric atomic ratio of the $NaYF_4$ product. ~1 mol% of Si component is detected, indicating that the surface SiO_2 has not been completely dissolved by HF (see 'reaction mechanism' section below) or the dissolved SiO_2 has been attached on the particle surface since the washing can not remove the Si ions completely.

Nitrogen adsorption-desorption isotherm displayed in Fig. 4 provides further evidence for the formation of the porosity within a large primary particle. The isotherm can be classified as a type IV, which is the characteristic of porous structure. The nitrogen adsorption-desorption measurement of the initial template $Y(OH)CO_3@SiO_2$ reveals no hysteresis-loop of nitrogen adsorption-desorption isotherm was observed (Figure S3, Supporting Information), implying that no mesopores exist in the initial template. This indicated that the reaction of $Y(OH)CO_3@SiO_2$ as a self-sacrificed template with Na^+ and F^- is an effective approach for the preparation of porous lanthanide fluoride materials with well-defined mesopores and controllable size and shape.

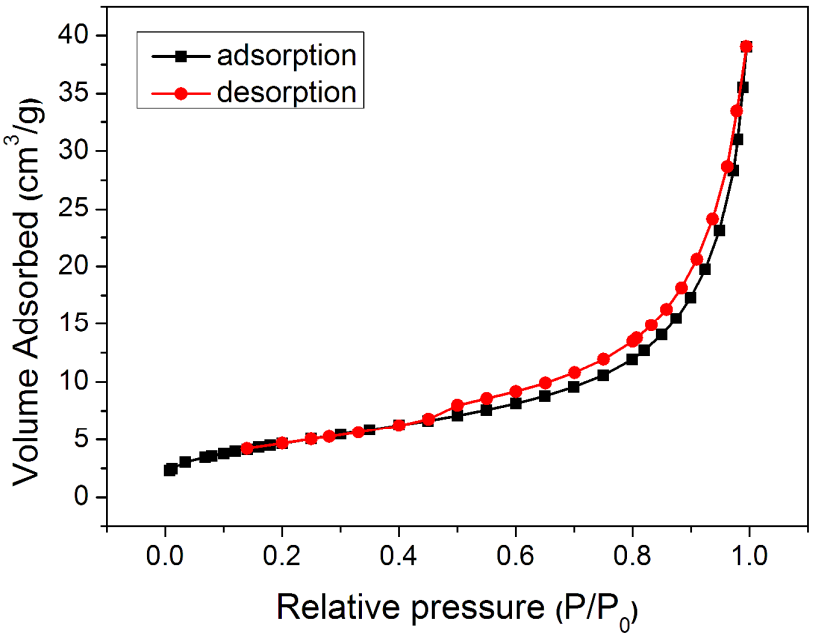

Fig. 4 Nitrogen absorption-desorption isotherms of the porous α-$NaYF_4$ particles synthesized by using $Y(OH)CO_3$@SiO_2 as self-sacrificed templates.

For comparison, we carried out a parallel experiment that the as-prepared precursor $Y(OH)CO_3$ microspheres without SiO_2 coating were hydrothermally reacted with $NaNO_3$ and NH_4F solutions under the same conditions above. XRD observation (Figure S4, Supporting Information) reveals that the product is also α-$NaYF_4$, but the size of the obtained particles is much larger than that of the initial template and no morphological homogeneity or porous structures were observed (Fig. 5). To explain such difference, it is essential for understanding the reaction mechanism involved in the overall reaction process.

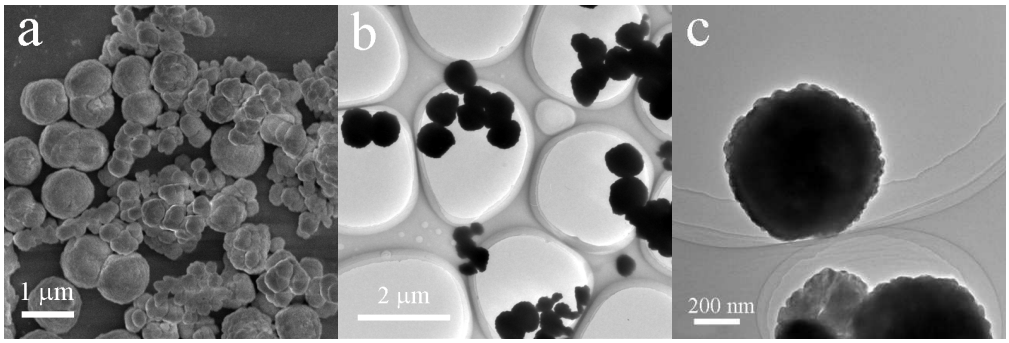

Fig. 5 SEM (a) and TEM images (b, c) of α-$NaYF_4$ particles synthesized by using the as-prepared precursor $Y(OH)CO_3$ as templates.

3.3. Reaction mechanism.

Scheme 1 schematically demonstrates the formation process of the porous microspheres composed of lots of α-$NaYF_4$ nanoparticles. First, the regular $Y(OH)CO_3$ microspheres were synthesized via a homogeneous precipitation progress. Upon the reaction with TEOS added, a thin silica layer was coated around $Y(OH)CO_3$ microspheres to form a core-shell $Y(OH)CO_3@SiO_2$ structure, which acted as a self-sacrificed template that itself was involved as a reactant source during the reaction. Upon the addition of NH_4F and $NaNO_3$ into $Y(OH)CO_3$ colloidal solution followed by a hydrothermal process, the reactions were involved as follows:

$$NH_4^+ + H_2O \leftrightharpoons NH_3{\cdot}H_2O + H^+ \quad (1)$$

$$Y(OH)CO_3 + H^+ \leftrightharpoons Y^{3+} + H_2O + CO_2 \quad (2)$$

$$Y^{3+} + Na^+ + 4F^- \rightarrow NaYF_4 \quad (3)$$

$$F^- + H_2O \leftrightharpoons HF + OH^- \quad (4)$$

$$SiO_2 + 4HF = SiF_4 + 2H_2O \quad (5)$$

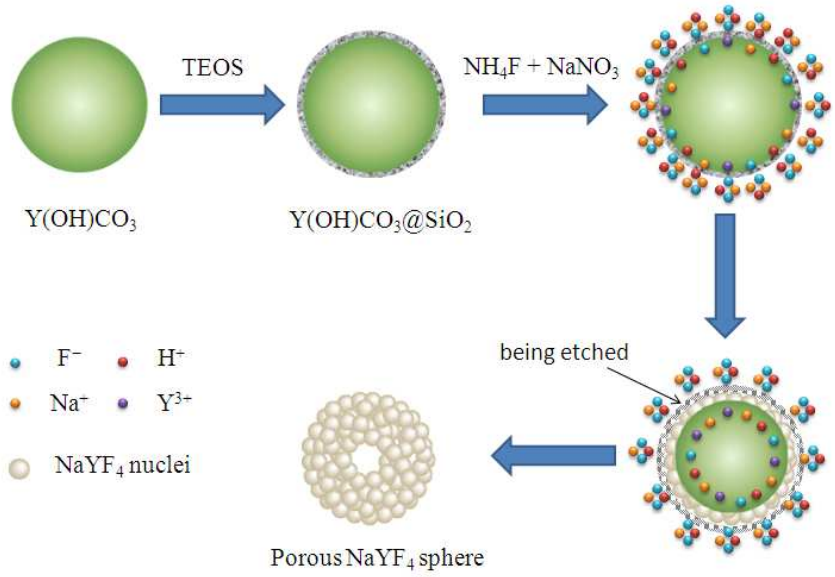

Scheme 1. Schematic demonstration of porous α-$NaYF_4$ microspheres via the reaction of $Y(OH)CO_3@SiO_2$ particles as a sacrificed template with NH_4F and $NaNO_3$ solutions.

In the initial stage of the reaction, H^+ ions generated as a result of the hydrolysis of NH_4^+ (1) were reacted with the $Y(OH)CO_3$ microsphere firstly at the $Y(OH)CO_3@SiO_2$ interface, thus releasing Y^{3+} ions (2), some of which were adsorbed

at the interface. Dissolving $NaNO_3$ and NH_4F in water could produce a number of Na^+ and F^- ions, respectively, some of which diffused towards the $Y(OH)CO_3@SiO_2$ interface and reacted with Y^{3+} ions to form the $NaYF_4$ nuclei (3). With the reaction progress, the inner of $Y(OH)CO_3$ microspheres was gradually corroded to produce more Y^{3+} ions, some of which migrated outward and reacted with Na^+ and F^- ions for the growth of the $NaYF_4$ nuclei, leading to the crystallization of α-$NaYF_4$ nanoparticles and the formation of interior voids in each newly formed microsphere. The mesopores were also created among these nanoparticles. Simultaneously, accompanied by α-$NaYF_4$ crystal growth, a slow dissolution process of SiO_2 shell by HF (see (4) and (5)) also occurred, leading to the gradual removal of surface SiO_2 layers.

As a matter of fact, the coated SiO_2 shell plays a key role in maintaining the size and shape and forming the porous structure in the finally formed product. On the one hand, Y^{3+} ions were produced and released, and Na^+ and F^- were penetrated into the $Y(OH)CO_3@SiO_2$ interfaces through SiO_2 shells, both with a low rate due to the presence of surface SiO_2 shell, which can slow down the overall reaction rate and improve the crystallization of $NaYF_4$. In addition, such slow etching process with SiO_2 protection allows for Y^{3+} migration and diffusion outward in long enough time, and thus forms a concentration gradient from the interior to exterior of a microsphere, leading to the formation of voids in the middle of each newly formed microsphere.

On the other hand, a majority of Y^{3+} ions produced cannot be escaped from the initial template particles due to the protection of surface SiO_2 shell around $Y(OH)CO_3$ microspheres. As a result, the reaction for the formation of $NaYF_4$ crystals occurs only within each single $Y(OH)CO_3@SiO_2$ microsphere, which can make the finally formed particles maintain almost the same size and shape with that of the original template.

However, for the $Y(OH)CO_3$ microspheres without SiO_2 coating as a reaction template, the bared $Y(OH)CO_3$ spheres were corroded with H^+ quickly, and the generated Y^{3+} and added Na^+ and F^- diffused with each other quickly due to the absence of surface protection shells. In addition, a few adjacent microspheres might be fused with each other easily also due to the absence of protection layers. This case

results in the size increase and inhomogeneity and no interior void formation for the finally formed particles. Therefore, $Y(OH)CO_3$ coated with SiO_2 shell provides a self-sacrificed template that serves not only as the reactant source, but also as a morphological controller. The formed α-$NaYF_4$ nanoparticles finally build up into a porous microsphere with the size and shape of original template based on a surface-protection etching and ion-exchange reaction mechanism.

3.4. Storage and release of fluorescence dye.

To study the storage and release behavior of our present single-phased porous α-$NaYF_4$ microspheres, Rhodamine 640 (Rh 640), a typical fluorescence dye, was chosen as a model dye to investigate the storage amount and efficiency. The porous mesoporous α-$NaYF_4$ microspheres were loaded with Rh 640 by soaking them in the Rh 640 aqueous solution. The dye-loaded particles were collected by centrifugation and washing three times followed by drying under vacuum. The absorptions of the original Rh 640 solution and the supernatant solution obtained by centrifugation were detected, respectively, and shown in Fig. 6a. We can see that the absorption intensity of the dye supernatant solution decreases gradually with soaking time. Up to 12 h a weak absorption was detected. For comparison, the dye loading experiment of $Y(OH)CO_3$@SiO_2 microspheres was also performed (Fig. 6b). A slight decrease in the dye absorption intensity was observed, compared to the case of porous α-$NaYF_4$ microspheres. Such parallel experiments demonstrated that our present porous α-$NaYF_4$ microspheres are capable to act as carriers with loading capability. The dye loading content can be evaluated by comparing the absorption of the supernatant solutions with that of original dye solution. Approximately 15 μg of dye molecules were stored inside 1 mg of hollow porous α-$NaYF_4$ particles. The loading efficiency of the dye was calculated as follows: $E\% = (O_{Dye}-R_{Dye})/O_{Dye}\times 100\%$, where O_{Dye} and R_{Dye} are the original and residual dye content, respectively. The dye loading efficiency was 87.09%, indicating a relatively high loading efficiency of our present porous materials.

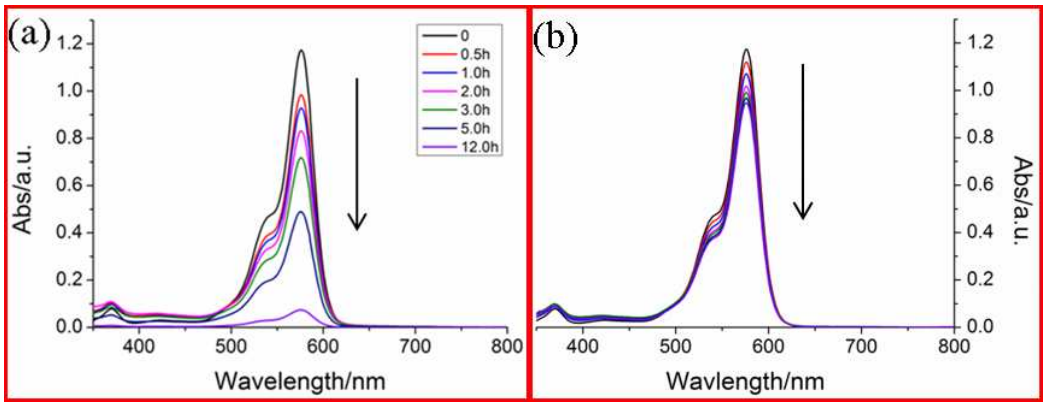

Fig. 6 UV-vis absorption spectra of Rh 640 solution treated with (a) porous α-$NaYF_4$ particles and (b) the as-prepared template $Y(OH)CO_3$@SiO_2 particles at selected time intervals in the dye storage process.

To verify the release behavior of dye-loaded particles, the particles were redispersed in aqueous solution at room temperature. Similarly, the absorption of released dye Rh 640 was measured at selected time intervals by using UV-vis absorption spectroscopy, as shown in Fig. 7, we can see that the absorption intensity of Rh 640 at ~576 nm increases gradually within 7 hours. For a clear comparison, the integrations of the absorption peaking at ~576 nm are shown in the inset of Fig. 7. By calculation, approximately 42.6% of the dye was released from mesopores within 7 h.

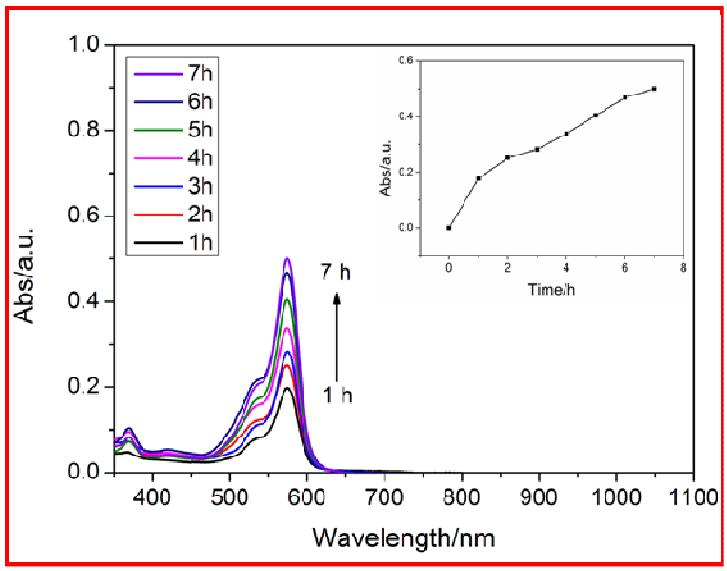

Fig. 7 UV-vis absorption spectra of the released Rh 640 loaded in the porous α-$NaYF_4$ particles at selected time intervals.

This indicates that the porous α-$NaYF_4$ microspheres loaded with dye possess a sustained release behavior. Such kinetics would be useful, especially for drug release for the treatment of cancer cells.[59] These results demonstrate that our present porous particles can be potentially used as an efficient carrier for specific uses such as in catalysis and therapy.[60−62]

3.5. Upconversion luminescence properties.

Rare earth fluorides have been shown to be efficient host lattices for upconversion luminescence (UCL) of lanthanide ions that can convert low-energy photons to high-energy ones.[40,41] In particular, cubic (α-) or hexagonal (β-) $NaYF_4$ has been reported as one of the most excellent infrared -to- violet/visible UCL host materials.[63−65] Here, (Yb^{3+}, Er^{3+}) and (Yb^{3+}, Tm^{3+}) ion pairs were respectively doped into porous α-$NaYF_4$ to investigate their UCL properties.

The UCL spectra of α-$NaYF_4$:18%Yb^{3+}, 2%Er^{3+} before and after annealing at 250°C were recorded under a 980 nm excitation and shown in Fig. 8a. The two primary bands in the green emission region with maxima at 521 and 543 nm can be assigned to the $^2H_{11/2} \rightarrow {}^4I_{15/2}$ and $^4S_{3/2} \rightarrow {}^4I_{15/2}$ transitions of the Er^{3+} ions, and the band at ~651 nm in the red emission region is assigned to the $^4F_{9/2} \rightarrow {}^4I_{15/2}$ transition of Er^{3+} ions.[66] The other emissions are also assigned in Fig. 8a.

It is worth noting that the ratio of green emission to red one was obviously changed for the samples before and after annealing. The red emission is slightly stronger than the green emission for the as-prepared sample α-$NaYF_4$:Yb^{3+},Er^{3+} while it is contrary for the sample annealed at 250°C. It is known that there are several factors that can influence the emission intensity, such as crystallographic phase, particle size and shape, concentration of rare earth ions, impurities and ligands. The characterizations for the annealed sample show that the sample annealed at 250°C is still α-$NaYF_4$ and the morphology of the particles has almost no change (Figure S5, Supporting Information). This indicates that the relative intensity change of green and red emissions for these two samples should be caused by another factor. As a matter of fact, for the α-$NaYF_4$:Yb^{3+},Er^{3+} sample without annealing, there exist a number of CO_3^{2-}, OH^- and H_2O on the particle surface due to the presence of Si−OH and the

dissolution of $Y(OH)CO_3$ in the reaction. The high vibration energies of these ions or molecules can easily relax the green-emitting levels ($^2H_{11/2}$ and $^4S_{3/2}$) to the red-emitting levels of Er^{3+} ($^4F_{9/2}$) via a nonradiative process (labeled with purple arrow, Fig. 8c).[67–70] It is known that CO_3^{2-}, OH^- and H_2O can be partially removed by annealing.[71] Thus, the different ratios of nonradiative relaxation in the two samples result in the variation of green-to-red ratio before and after annealing. Therefore, the emission color of doped upconverting luminescence materials can be modulated by controlling the amount of CO_3^{2-} or OH^- acting as nonradiative recombination centers.

Fig. 8b shows the UCL spectrum of α-$NaYF_4$:20%Yb^{3+}, 1%Tm^{3+} under a 980 nm laser excitation. α-$NaYF_4$ co-doped with Yb^{3+} and Tm^{3+} ions emit UV and visible light. UV emission peaks centered at 291 nm, 349 nm, and 362 nm are assigned to the transitions of Tm^{3+} ions: $^1I_6 \rightarrow {}^3H_6$, $^1I_6 \rightarrow {}^3F_4$, and $^1D_2 \rightarrow {}^3H_6$, respectively. Two blue emission peaks centered at 450 nm and 474 nm are assigned to $^1D_2 \rightarrow {}^3F_4$ and $^1G_4 \rightarrow {}^3H_6$ transitions of Tm^{3+} ions, respectively. The relatively weak emissions at ~ 645 nm and ~ 804 nm are assigned to $^1G_4 \rightarrow {}^3F_4$ and $^3H_4 \rightarrow {}^3H_6$ transitions of Tm^{3+} ions, respectively.[72] Similarly, the UV-to-visible emission ratio was also markedly varied for Yb-Tm-codped α-$NaYF_4$ before and after annealing, which was explained by the same reason in the case of Yb-Er-codped α-$NaYF_4$.

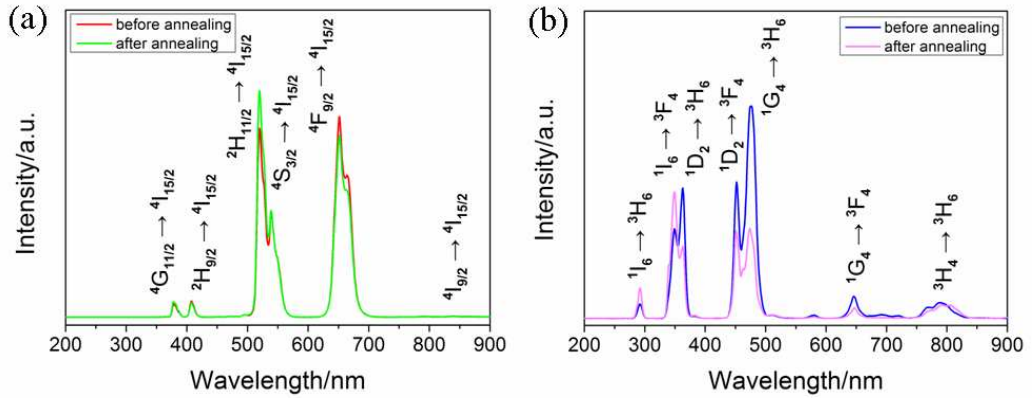

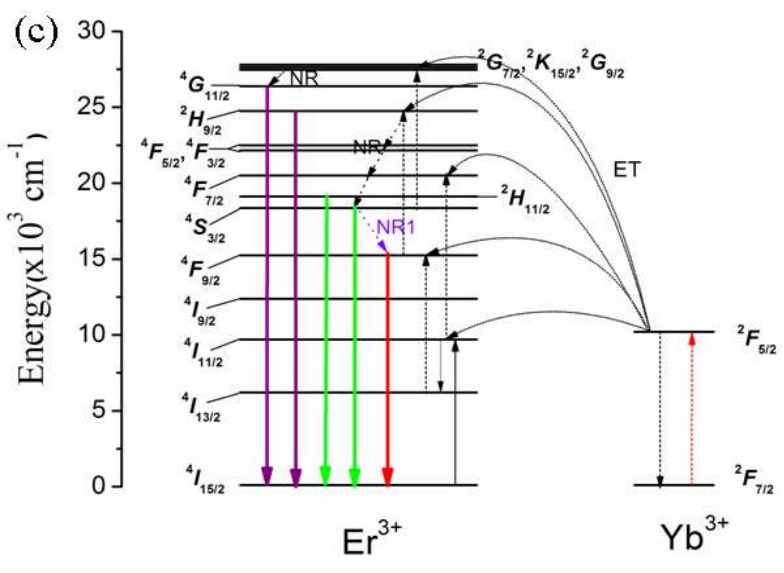

Fig. 8 UC emission spectra of the porous structured $NaYF_4$:Yb^{3+},Er^{3+} (a) and $NaYF_4$:Yb^{3+},Tm^{3+} (b) and diagram of energy levels of Yb^{3+}-Er^{3+} and upconversion luminescence processes in an Yb^{3+}-Er^{3+} codoped system under 980 nm excitation (c).

4. Conclusion

In this paper, the $Y(OH)CO_3·H_2O$ microspheres with a diameter of ~260 nm were synthesized via a general urea-based homogeneous precipitation process. The silica with a thickness of ~8 nm was homogeneously coated around $Y(OH)CO_3·H_2O$ microspheres by a sol-gel method. The formed $Y(OH)CO_3$@SiO_2 particles were used as a sacrificed template, which not only acts as the morphological controller, but also as the reactant source of Y^{3+} for the formation of cubic-phased (α-) $NaYF_4$ upon the reaction with NH_4F and $NaNO_3$ solutions. SEM, TEM and N_2 adsorption-desorption characterizations revealed that the finally formed porous α-$NaYF_4$ microspheres are composed of hundreds of nanoparticles and maintain the size and shape of the original template. Compared with the parallel experiment carried out on the bared $Y(OH)CO_3$ microspheres as reaction template, the SiO_2 shell was indicated to play a vital role in the size and shape control and porosity formation. We believed that the reaction mechanism is based on a surface-protected etching and ion-exchange reaction process. The dye loading and release in the finally formed porous α-$NaYF_4$ microspheres were

investigated using Rhodamine 640 as a model dye, showing a relatively high loading content and a sustained release ratio. Under 980 nm NIR excitation, (Yb^{3+}, Tm^{3+}) and (Yb^{3+}, Er^{3+}) co-doped α-$NaYF_4$ porous phosphors showed bright blue- and green-emitting upconversion luminescence, respectively. Therefore, our present porous α-$NaYF_4$:Ln^{3+} have potential applications in drug deliver and cell imaging by combining upconversion luminescence properties and storage and release behaviors.

Acknowledgment

We acknowledge financial support from the National Science Foundation of China (Grant No. 61178073).

References

1 Y. Chen, H. R. Chen, D. P. Zeng, Y. B. Tian, F. Feng, J. W. Chen and J. L. Shi, *ACS Nano*, 2010, **4**, 6001.

2 X. W. Lou, L. A. Archer and Z. C. Yang, *Adv. Mater.*, 2008, **20**, 3987.

3 A. B. Bourlions, M. A. Karakassides and D. Petridis, *Chem. Commun.*, 2001, 1518.

4 P. P. Yang, Z. W. Quan, Z. Y. Hou, C. X. Li, X. J. Kang, Z. Y. Cheng and J. Lin, *Biomaterials*, 2009, **30**, 4786.

5 X. M. Sun, J. F. Liu and Y. D. Li, *Chem. Eur. J.* 2006, **12**, 2039.

6 L. N. Kong, N. Wei, Q. F. Zhao, J. Q. Wang and Y. Wan, *ACS Catal.*, 2012, **2**, 2577.

7 Y. Kim, J. B. Jeon and J. Y. Chang, *J. Mater. Chem.*, 2012, **22**, 24075.

8 S. A. EI-Safty, M. A. Shenashen, M. Ismael, M. Kairy and M. R. Awual, *Analyst*, 2012, **137**, 5278.

9 P. Prarat, C. Ngamcharussrivichai, S. Khaodhiar and P. J. Punyapalakul, *Hazar. Mater.*, 2013, **244**, 151.

10 Y. Chen, H. R. Chen, S. J. Zhang, F. Chen, L.X. Zhang and J. M. Zhang, *Adv. Funct. Mater.*, 2011, **21**, 270−278.

11 X. F. Yu, D. S. Wang, Q. Peng and Y. D. Li, *Chem. Commun.*, 2011, **47**, 8094.

12 J. Kim, H. S. Kim, N. Lee, T. Kim, H. Kim, T. Yu, I. C. Song, W. K. Moon and T. Hyeon, *Angew. Chem. Int. Ed.*, 2008, **47**, 8438.

13 M. Liong, J. Lu, M. Kovochich, T. Xia, S. G. Ruehm, A. E. Nel, F. Tamanoi and J. I. Zink, *ACS Nano*, 2008, **2**, 889.

14 J. E. Lee, N. Lee, H. Kim, J. Kim, S. H. Choi, J. H. Kim, T. Kim, I. C. Song, S. P. Park, W. K. Moon and T. Hyeon, *J. Am. Chem. Soc.*, 2010, **132**, 552.

15 B. G. Trewyn, S. Giri, I. I. Slowing and V. S.-Y. Lin, *Chem. Commun.*, 2007, 3236.

16 J. M. Rosenholm, C. Sahlgren and M. Lindén, *Nanoscale*, 2010, **2**, 1870.

17 W. H. Di, X. G. Ren, H. F. Zhao, N. Shirahata, Y. Sakka and W. P. Qin, *Biomaterials*, 2011, **32**, 7226.

18 Y. Q. Wang, G. Z. Wang, H. Q. Wang, C. H. Liang, W. P. Cai and L. D. Zhang, *Chem. Eur. J.*, 2010, **45**, 3497.

19 R. A. Jalil and Y. Zhang, *Biomaterials*, 2008, **29**, 4122.

20 S. Jiang, K. Y. Win, S. H. Liu, C. P. Teng, Y. G. Zheng and M. Y. Han, *Nanoscale*, 2013, **5**, 3127.

21 Y. S. Li, J. L. Shi, Z. L. Hua, H. R. Chen and M. L. Ruan, *Nano Lett.*, 2003, **3**, 609.

22 A. M. Collins, C. Spickermann and S. Mann, *J. Mater. Chem.*, 2003, **13**, 1112.

23 Q. Peng, Y. J. Dong and Y. D. Li, *Angew. Chem. Int. Ed.*, 2003, **42**, 3027.

24 A. Wolosiuk, O. Armagan and P. V. Braun, *J. Am. Chem. Soc.*, 2005, **127**, 16356.

25 L. Z. Wang, Y. Ebina, K. Takada and T. Sasaki, *Chem. Commun.*, 2004, 1074.

26 Y. D. Xia and R. Mokaya, *J. Mater. Chem.*, 2005, **15**, 3126.

27 P. Jiang, J. F. Bertone and V. L. Colvin, *Science*, 2001, **291**, 453.

28 X. Guo and F. Szoka, *Acc. Chem. Res.*, 2003, **36**, 355.

29 M. H. Oh, T. Yu, S. H. Yu, B. Lim, K. T. Ko, M. G. Willinger, D. H. Seo, B. H. Kim, M. G. Cho, J. H. Park, K. Kang, Y. E. Sung, N. Pinna and T. Hyeon, *Science*, 2013, **340**, 964.

30 G. Z. Chen, F. Rosei and D. L. Ma, *Adv. Funct. Mater.*, 2012, **22**, 3914.

31 G. Z. Chen, S. X. Sun, W. Zhao, S. L. Xu and T. You, *J. Phys. Chem. C.*, 2008, **112**, 20217.

32 W. Li, F. Zhang, Y. Q. Dou, Z. X. Wu, H. J. Liu, X. F. Qian, D. Gu, Y. Y. Xia, B. Tu and D. Y. Zhao, *Adv. Energy Mater.*, 2011, **1**, 382.

33 Y. D. Yin, R. M. Rioux, C. K. Erdonmez, S. Hughes, G. A. Somorjai and A. P. Alivisator, *Science*, 2004, **304**, 711.

34 B. Liu and H. C. Zeng, *J. Am. Chem. Soc.*, 2004, **126**, 16744.

35 F. Zhang, Y. F. Shi, X. H. Sun and D. Y. Zhao, *Chem. Mater.*, 2009, **21**, 5237.

36 G. Cheng, J. L. Zhang, D. H. Sun and J. Z. Ni, *Chem. Eur. J.*, 2012, **18**, 2014.

37 L. H. Zhang, M. L. Yin, H. P. You, M. Yang, Y. H. Song and Y. J. Huang, *Inorg. Chem.*, 2011, **50**, 10608.

38 X. Y. Yang, Y. Zhang, L. Xu, Z. Zhai, M. Z. Li, X. L. Liu and W. H. Hou, *Dalton Trans.*, 2013, **42**, 3986.

39 J. F. Suyver, A. Aebischer, D. Biner, P. Gerner, J. Grimm, S. Heer, K. W. Krämer, C. Reinhard and H. U. Güdel, *Opt. Mater.*, 2005, **27**, 1111.

40 F. Wang, R. R. Deng, J. Wang, Q. X. Wang, Y. Han, H. M. Zhu, X. Y. Chen and X. G. Liu, *Nat. Mater.*, 2011, **10**, 968.

41 X. F. Yu, M. Li, M. Y. Xie, L. D. Chen, Y. Li and Q. Q. Wang, *Nano Res.*, 2010, **3**, 51.

42 G. S. Yi, H. C. Lu, S. Y. Zhao, G. Yue, W. J. Yang, D. P. Chen and L. H. Guo, *Nano Lett.*, 2004, **4**, 2191.

43 D. K. Chatterjee, A. J. Rufaihah and Y. Zhang, *Biomaterials*, 2008, **29**, 937.

44 F. Wang, Y. Han, C. S. Lim, Y. H. Lu, J. Wang, J. Xu, H. Y. Chen, C. Zhang, M. H. Hou and X. G. Liu, *Nature*, 2010, **463**, 1061.

45 J. Wang, R. R. Deng, M. A. MacDonald, B. L. Chen, J. K. Yuan, F. Wang, D. Z. Chi, T. S. A. Hor, P. Zhang, G. K. Liu, Y. Han and X. G. Liu, *Nat. Mater.*, 2013, DOI:10.1038/nmat3804.

46 X. M. Li, D. K. Shen, J. P. Yang, C. Yao, R. C. Che, F. Zhang and D. Y. Zhao, *Chem. Mater.*, 2013, **25**, 106.

47 C. Zhang and J. Y. Lee, *ACS Nano*, 2013, **7**, 4393.

48 F. Zhang, R. C. Che, X. M. Li, C. Yao, J. P. Yang, D. K. Shen, P. Hu, W. Li and D. Y. Zhao, *Nano Lett.*, 2012, **12**, 2852.

49 Y. Wu, D. M. Yang, X. J. Kang, P. A. Ma, S. S. Huang, Y. Zhang, C. X. Li and J. Lin, *Dalton Trans.*, 2013, **42**, 9852.

50 Y. H. Han, S. L. Gai, P. A. Ma, L. Z. Wang, M. L. Zhang, S. H. Huang and P. P. Yang, *Inorg. Chem.*, 2013, **52**, 9184.

51 F. Wang, D. Banerjee, Y. S. Liu, X. Y. Chen and X. G. Liu, *Analyst* 2010, **135**, 1839.

52 Y. S. Liu, D. T. Tu, H. M. Zhu, R. F. Li, W. Q. Luo and X. Y. Chen, *Adv. Mater.*, 2010, **22**, 3266.

53 L. L. Li, R. B. Zhang, L. L. Yin, K. Z. Zheng, W. P. Qin, P. R. Selvin and Y. Lu, *Angew. Chem. Int. Ed.*, 2012, **51**, 6121.

54 F. Zhang, Y. F. Shi, X. H. Sun, D. Y. Zhao and G. D. Stucky, *Chem. Mater.*, 2009, **21**, 5237.

55 E. Matijević and W. P. Hsu, *J. Colloid Interface Sci.*, 1987, **118**, 506.

56 J. G. Li, X. D. Li, X. D. Sun, T. Ikegami and T. Ishigaki, *Chem. Mater.*, 2008, **20**, 2274.

57 W. H. Di, S. K. P. Velu, A. Lascialfari, C. X. Liu, N. Pinna, P. Arosio, Y. Sakka and W. P. Qin, *J. Mater. Chem.*, 2012, **22**, 20641.

58 H. S. Cho, Z. Y. Dong, G. M. Pauletti, J. M. Zhang, H. Xu, H. C. Gu, L. M. Wang, R. C. Ewing, C. Huth, F. Wang and D. L. Shi, *ACS Nano*, 2010, **4**, 5398.

59 Y. Zhu, T. Ikoma, N. Hanagata and S. Kaskel, *Small*, 2010, **6**, 471.

60 J. Baek, H. J. Yun, D. Yun, Y. Choi and J. Yi, *ACS catal.*, 2012, **2**, 1893.

61 Y. Zhang, E. C. Judkins, D. R. McMillin, D. Mehta and T. Ren, *ACS catal.*, 2013, **3**, 2474.

62 H. Qian, H. Guo, P. Ho, R. Mahendran and Y. Zhang, *Small*, 2009, **5**, 2285.

63 L. Y. Wang, and Y. D. Li, *Chem. Mater.*, 2007, **19**, 727.

64 F. Wang, and X. G. Liu, *Chem. Soc. Rev.*, 2009, **38**, 976.

65 J. C. Boyer, F. Vetrone, L. A. Cuccia and J. A. Capobianco, *J. Am. Chem. Soc.*, 2006, **128**, 7444.

66 T. Y. Cao, T. S. Yang, Y. Gao, Y. Yang, H. Hu and F. Y. Li, *Inorg. Chem. Commun.*, 2010, **13**, 392.

67 J. M. Nedelec, D. Avignant and R. Mahiou, *Chem. Mater.*, 2002, **14**, 651.

68 H. Maas, A. Currao and G. Calzaferri, *Angew. Chem. Int. Ed.*, 2002, **41**, 2495.

69 K. Rajesh, P. Mukundan, P. Krishana Pillai, V. R. Nair and K. G. K. Warrier, *Chem. Mater.*, 2004, **16**, 2700.

70 S. L. Wu, Y. H. Ning, J. Chang, W. B. Niu and S. F. Zhang, *Cryst. Eng. Comm.*, 2013, **15**, 3919.

71 W. H. Di, X. J. Wang, B. J. Chen, S. Z. Lu and X. X. Zhao, *J. Phys. Chem. B*, 2005, **109**, 13154.

72 H. Chen, X. S. Zhai, D. Li, L. L. Wang, D. Zhao and W. P. Qin, *J. Alloys Compd.*, 2012, **511**, 70.

For Table of Contents Use Only

Synthesis of porous upconverting luminescence α-$NaYF_4$:Ln microspheres and their potential application as carriers

Changjian Lv, Weihua Di*, Zhihe Liu, Kezhi Zheng, and Weiping Qin*